

# Switching exploration modes in human mobility

Lu Zhong<sup>1,2,6</sup>, Lei Dong<sup>3,6</sup>, Qi Wang<sup>4</sup>, Chaoming Song<sup>5</sup>, Jianxi Gao<sup>1,2\*</sup>

<sup>1</sup>*Department of Computer Science, Rensselaer Polytechnic Institute, Troy, NY, USA*

<sup>2</sup>*Network Science and Technology Center, Rensselaer Polytechnic Institute, Troy, NY, USA*

<sup>3</sup>*Institute of Remote Sensing and Geographical Information Systems, School of Earth and Space Sciences, Peking University, Beijing, China*

<sup>4</sup>*Department of Civil and Environmental Engineering, Northeastern University, Boston, MA, USA*

<sup>5</sup>*Department of Physics, University of Miami, Coral Gables, FL, USA*

<sup>6</sup>*These authors contributed equally: Lu Zhong, Lei Dong.*

*Email: gaoj8@rpi.edu*

**Recent advances in human mobility research have revealed consistent pairwise characteristics in movement behavior, yet existing mobility models often overlook the spatial and topological structure of mobility networks. By analyzing millions of devices' anonymized cell phone trajectories, we uncover a distinct modular organization within these networks, demonstrating that movements within spatial modules differ significantly from those between modules. This finding challenges the conventional assumption of uniform mobility dynamics and underscores the influence of heterogeneous environments on human movement. Inspired by switching behaviors in animal movement patterns, we introduce a novel "switch mechanism" to differentiate movement modes, allowing our model to accurately reproduce both the modular structures of trajectory networks and spatial mobility patterns. Our results provide**

**new insights into the dynamics of human mobility and its impact on network formation, with broad applications in traffic prediction, disease transmission modeling, and urban planning. Beyond advancing the theoretical and practical understanding of mobility networks, this work opens new avenues for understanding societal dynamics at large.**

## **Introduction**

Understanding human daily mobility has been crucial for a multitude of applications<sup>1</sup>, and over the past two decades, significant advancements have been made in uncovering shared regularities in human movement<sup>2</sup>. These discoveries encompass phenomena such as Lévy flights<sup>3,4</sup>, the distribution of time allocation<sup>5</sup>, visit frequencies<sup>6</sup>, exploration tendencies and return regularities<sup>7,8</sup>, and inflation pattern<sup>9</sup>, which have led to advances in human mobility models<sup>1,10–13</sup>. However, when comparing the real data with the classical model, we find that the spatial and topological structure of the mobility network generated by the widely used human mobility model (EPR model) is very different from the real data (Fig. 1a-d). Specifically, the stay points of users in real data are more spatially dispersed, bringing higher average shortest-path length and modularity in network metrics (Fig. 1ef). At the mesoscale, the frequency of people's trips decreases with distance from home, but the decay rate is significantly lower than the model predictions (i.e., people make substantial trips far from home, Fig. 1g). These inconsistencies suggest that our current understanding of human mobility is missing some important mechanisms.

As a mobile species, humans share many similarities with animals in movement patterns, and studies of animal mobility in recent years have found different mobility modes across natural

areas<sup>14-17</sup>. For instance, due to resource patchiness, avians switch between a wide-ranging commuting mode of movement across patches and an intensive, area-restricted searching mode for prey within a local patch<sup>14,15</sup>. The observed switch behavior inspires us to consider whether this mechanism also exists for human mobility and whether it happens to explain the inconsistency between the model and the data, as shown in Fig. 1. In fact, cities share many similarities with natural areas that feature distinct clusters of resources (such as amenities and employment opportunities)<sup>18-21</sup>. The mobility mode within and across spatial clusters of resources may be diverse.

To systematically test our hypothesis, we analyzed two large-scale cell phone datasets. One dataset consists of six months of privacy-enhanced GPS trajectory data collected from two million anonymized users in the United States, while the other includes two weeks of call detail records from 300,000 anonymized users in Senegal(see Methods and Figs. S1). By constructing mobility networks from cell phone trajectories, we detect a polycentric modular structure of the network and find users exhibiting similar intra-module exploration modes but differing inter-module exploration modes. Leveraging these insights, we introduce a switch mechanism to differentiate the exploration mode. This mechanism not only allows for precise replication of individual trajectories but also illustrates the emergence of polycentric structures within the trajectory networks. The introduction of the switch mechanism opens new avenues for predicting mobility flows, particularly in long-range movements, which is vital for accurate disease spread forecasting.

## Results

**Polycentric module structure in human mobility network.** To characterize the structure of mobility data, we construct human trajectory networks based on cell phone data, where stay points as network nodes and paths connecting consecutive stay points are edges. The reciprocal of the spatial distance between stay points defines the edge weights. Hence, a smaller spatial distance results in a greater edge weight (see Methods). Figures 1a and c display a trajectory of a real user and the corresponding mobility network, which has a polycentric structure with several activity regions. Comparing the empirical mobility network with the network generated by the classical exploration and preferential return (EPR) model, it is clear that the real-world mobility network manifests multiple modules. Conversely, the EPR model typically generates a single, highly connected module centered around the home location. Consequently, real-world mobility networks have significantly longer topological paths than the model, as shown in Fig. 1e and Extended Data Fig. 1. In terms of network metrics, the EPR model typically exhibits a two-degree separation (the average shortest path length is two), implying that an individual can traverse any pair of locations through a single central transit hub. In contrast, real-world mobility networks' average shortest-path length follows a normal distribution with a median value of nearly four, implying a four-degree separation.

To quantify the observed polycentricity of the mobility network, we use geometric modularity ( $Q$ ), which serves as a measure of the extent to which a network can be partitioned into distinct modules<sup>22</sup>. Figure 1f shows that the modularity of individual mobility networks exhibits a consid-

erably high median value  $Q$  around 0.66. This is in contrast to the EPR model, which demonstrates lower modularity, with a median value of 0.28. This higher value from empirical data suggests a high degree of segmentation of human mobility into multiple modules. In addition to the network metrics, the mesoscopic mobility patterns observed in the empirical data displayed in Fig. 1g show notable differences with models, with significantly a broader tail for distant trips that are far from home. This distinct difference arises from the occurrence of long-range travels across modules, a feature conspicuously absent from previous models. See Extended Data Fig.1 for the results of Senegal mobility networks and Fig. S2-S3 for other details.

**Switch of exploration mode.** Our analysis of the mobility patterns reveals a polycentric modular structure, wherein locations within a module are spatially and topologically proximate, while intra-module travel requires significant displacement. We apply the Louvain method to extract modules from individual trajectory networks. The trajectory is then divided into two types of travel: intra-module travels, which involve movement within the local built environment, and inter-module travels, which refer to movement between different modules. After extracting the modules from the mobility network, as shown in Fig. 2a, the user switches between intra-module and inter-module travels with switch tendency  $P_{Switch}$ .

To examine whether the dynamics of mobility behavior within modules differs with that across modules, we employ the mean square displacement (MSD). The MSD is defined as the squared displacement of an individual's position with regard to the reference position over time. Previous research suggests  $MSD(t)^{1/2} \sim \log(t)^v$ , indicating subdiffusive dynamics and a strong

tendency to revisit familiar places <sup>7</sup>. A lower value of  $v$  indicates a stronger propensity to return (smaller tendency to explore). As depicted in Fig. 2b-d, the growth rate  $v$  for intra-module movement differs from that for inter-module movement, challenging prior studies that assume uniform  $v$  across all spatial scales. To determine if the growth rate  $v$  is consistent among individuals, we classify users by their radius of gyration  $R_{gc}$ . Figure 2d illustrates that, while the growth rate  $v$  for intra-module movements remains relatively stable, the rate for inter-module movements increases for users with a larger  $R_{gc}$ . See Fig. S4 for the results for Senegal data.

To calibrate the switch in mobility behavior, we measure the tendencies for exploration and return,  $P_w$  and  $1 - P_w$  for within-module movements, and  $P_c$  and  $1 - P_c$  for between-module movements, respectively. The exploration tendency  $P_w$  ( $P_c$ ) is calculated as the proportion of unique locations (module) visited relative to the total movements within a module (cross modules). Figures S4-S5 demonstrate that  $P_w \sim S_w^{-\gamma_w}$  and  $P_c \sim S_c^{-\gamma_c}$ , whereas the  $\gamma_w$  consistent across users with different radii of gyration ( $R_{gc}$ ), but  $\gamma_c$  decreases for users with higher radii of gyration. It indicates that the tendency to explore within modules is similar across users, but the tendency to explore across modules increases with larger  $R_{gc}$ , same as demonstrated in Fig. 2e.

**Predictions of switch mechanism.** Building on the identified behavior, we introduce the switch mechanism and the calibrated parameters into the standard exploration/preferential return scheme model <sup>7</sup> (see Methods and Fig. S6-S8). As shown in Fig. 1, our switch model accurately depicts the characteristics of mobility networks. The model's projection of the average path length aligns closely with empirical data, with a median value of approximately  $L_{\text{Switch}} = 3.78$  (Fig. 1e). More-

over, our model captures the modular structure observed in empirical mobility networks. As shown in Fig. 1 and Extended Data Fig. 1, our model yields a high modularity measure, closely matching empirical findings with  $Q_{\text{Switch}} = 0.68$  for U.S. data and  $Q_{\text{Switch}} = 0.35$  for Senegal data. This stands in sharp contrast to the smaller modularity offered by the EPR model, with  $Q_{\text{EPR}} = 0.28$  for U.S. data and  $Q_{\text{EPR}} = 0.20$  for Senegal data. For the clustering coefficient, indicative of a propensity for triangle paths, our model results align with empirical values ( $C_{\text{Switch}} = 0.31$  for U.S. data and  $C_{\text{Switch}} = 0.32$  for Senegal data). The EPR model, in contrast, predicts higher clustering coefficients ( $C_{\text{EPR}} = 0.38$  for U.S. data and  $C_{\text{EPR}} = 0.53$  for Senegal data).

Contrary to conventional network science beliefs, where high modularity typically results in a larger clustering coefficient and vice versa<sup>23</sup>, we observe an unusual negative correlation between modularity and clustering coefficient in mobility networks. This observation uncovers a key aspect of the polycentric nature of human mobility networks, further underscoring the validity of our model. Such a negative correlation embodies the polycentric modular structure of human mobility networks, where each module has a star-like structure dominated by a few transit hubs. These hubs route most paths, leaving few opportunities for triangle formation, thereby, resulting in a low clustering coefficient. At the same time, the high degree of module separation results in high modularity. The distinct contrast between our model and the traditional egocentric EPR model becomes particularly apparent in the scatter plot of modularity versus clustering coefficient, as depicted in Fig. 3. Our proposed model and the empirical data it represents occupy the bottom-right corner of the plot, symbolizing a combination of high modularity and low clustering coefficient. In stark contrast, the egocentric EPR model, represented by a single, highly interconnected module,

occupies the top-left corner, corresponding to low modularity and a high clustering coefficient.

Furthermore, our model better predicts long-range movements. Figure 1g shows that our model fits with empirical data in capturing travels that are distant from home. After integrating all users' travels, we show that our model also exhibits superior agreement with empirical data in county-level mobility fluxes, particularly in long-range mobility trips, as illustrated in Fig. 4a-c and Extended Data Fig. 2. The polycentric nature of the mobility network generated by our model enables a direct connection between two distant counties. In contrast, the egocentric EPR model tends to overestimate short-range fluxes, thereby failing to reproduce direct long-range connections. On the predicted and empirical mobility fluxes, we simulate the disease spread using a meta-population model (see Methods for details of the simulation). Our model excels in predicting the spread of disease, while the EPR model overestimates local infections and underestimates infections distant from sources. This discrepancy is evident in the example comparison at the same time shown in Fig. 4d. When evaluating the overall progression of infections over time in Fig. 4e, our model consistently outperforms the EPR model with prediction errors up to four times lower.

## **Discussion**

Our study shows the nuanced dynamics of human mobility, particularly identifying the switch of exploration modes across spatial scales and diverse populations. The underlying mechanisms contribute to the uniqueness of the human trajectory network, characterized by high modularity and clustering, leading to a polycentric nature where each module contains a hub. By categorizing



users according to various demographic factors, including age, gender, race, ethnicity, poverty level, and household income (Extended Data Fig. 3), we found that the modular structure and the topological features of the trajectory network remained consistent regardless of variations in individual demographics.

The switch mechanism highlights the impact of heterogeneous distributions and clustered resources in urban environments on human mobility<sup>19–21</sup>. It reveals how humans switch between long-range, cross-module travel modes and short-range, within-module travel modes to meet daily human needs such as food, social interactions, and other necessities. The model’s ability to accurately predict both individual and collective mobility patterns presents significant potential for future practical applications, particularly in urban planning<sup>24</sup>, epidemic prevention<sup>25,26</sup>, and mitigating activity inequality<sup>27–29</sup>.

Moreover, the switch mechanism aligns with fundamental principles observed in animal and molecular movement<sup>14,15,30</sup>, as well as key concepts in movement ecology<sup>16,31</sup>. This cross-disciplinary connection broadens the scope of our model, suggesting its potential utility across diverse research domains. Future efforts could focus on refining the model to address specific scenarios or integrating it with complementary approaches to enhance its applicability. These insights not only highlight the importance of understanding mobility patterns at multiple scales but also open avenues for collaborative studies across disciplines to tackle pressing challenges in movement dynamics and beyond.

## Methods

**Data.** We analyzed human movement using two datasets: the U.S. dataset from Cuebiq Inc. and the Senegal dataset from the D4D Senegal Challenge<sup>6,32</sup>. The U.S. dataset contains anonymized location data of 42 million devices from January to June 2020. All devices opted into anonymized data collection for research purposes. In addition to de-identifying the data, the data provider also obfuscates home locations to the census block group level to preserve privacy. Using the Infostop algorithm<sup>33</sup>, we processed this data to identify stay points, focusing on 2.1 million users with over thirty days of data. We divided the dataset based on the pre and post-lockdown periods starting March 11, 2020, mainly using the pre-lockdown data for analysis and validation with the post-lockdown segment. The Senegal dataset comprises anonymized call records from 2013, segmented into 25 two-week periods with about 44 million records from 300,000 users, capturing movement linked to mobile towers. Table. S1 summarizes the basic statistics of the two datasets.

For the data preprocessing, we categorize the geographical locations of all users by employing the H3 indexing system at a resolution of 12. This system divides the physical space into hexagonal cells, each with an edge length of roughly 9 meters. We determine users' home locations based on the cell they visit most frequently during the night, specifically between 8 p.m. and 8 a.m.

**Characterizing human trajectory networks.** For each user's sequence of stay points  $T = \{\theta_1, \dots, \theta_i, \dots\}$  where  $i$  indexes the sequence, we construct the trajectory network  $G(T)$ . In this network, nodes represent stay points, and edges correspond to consecutive travels between these points. To ensure

that all weights are non-negative and that shorter distances between points yield larger weights, we define the edge weight between two consecutive points  $(\theta_i, \theta_{i+1})$  as  $w(\theta_i, \theta_{i+1}) = \log(\frac{\hat{d}}{d(\theta_i, \theta_{i+1})})$ , where  $d(\theta_i, \theta_{i+1})$  represents the spatial distance between consecutive stay points, and  $\hat{d}$  is a pre-defined maximum jump distance. This inverse distance weighting reflects Tobler's first law of geography<sup>34</sup>, suggesting that closer entities have stronger spatial interactions. We set  $\hat{d}$  as 4,000km for the U.S. and 1,000km for Senegal.

To analyze the trajectory network, we calculate key metrics<sup>35</sup> such as the shortest path length ( $L$ ), average clustering coefficient ( $C$ ), and weighted modularity<sup>23</sup> ( $Q$ ). For the detection of modules within the weighted directed trajectory network  $G(T)$ , we employ the Louvain method<sup>36</sup>. This method helps identify sub-networks, or modules, composed of stay points that are closely linked both spatially and topologically.

**Characterizing mobility dynamics within and across modules.** Building on existing studies, we characterize mobility dynamics within and between modules by calculating the mean square displacement (MSD). MSD measures the squared deviation of an individual's position from a reference position, averaged across various movement paths, defined as  $\text{MSD}(t) = \langle \Delta x^2(t) \rangle$ . If the movement is superdiffusive, then  $\langle \Delta x^2(t) \rangle \sim t^v$  with  $v > 1$ . In the case of Brownian motion,  $\langle \Delta x^2(t) \rangle \sim t^v$  with  $v = 1$ . However, for subdiffusive dynamics,  $v < 1$ . For both intra-module and inter-module mobility behaviors, we find that:

$$\text{MSD}(t)^{1/2} \sim \log(t)^v \quad (1)$$

This relationship indicates that MSD follows a growth slower than logarithmic, suggesting an ultraslow diffusive process. Moreover, the growth rates  $v$  vary between intra-module and inter-module behaviors. Larger growth rates  $v$  suggest a higher (lower) likelihood of exploring new locations (returning to familiar locations).

**Switch mechanism.** We introduce the switch mechanism to the typical individual mobility model, i.e., the EPR model<sup>7</sup>, to account for the difference in intra- and inter-module mobility behaviors. As illustrated in Fig. S6, users with a unique radius of gyration  $R_{gc}$  will initiate their first move from their home locations. After a waiting time  $\Delta t$ , we assume that the user who is at module  $i$  has the probability of  $P_{Switch}$  of switching inter-module mode or  $1 - P_{Switch}$  to continue stay in current module  $i$  :

Option (1): Inter-module mode. The individual may either transition to a new module  $j$  with a probability  $P_c$  or return to a frequently visited module with a probability  $1 - P_c$ . The count of inter-module movements  $n_c$  increases to  $n_c + 1$ . Should they venture into a new module, the count of unique modules visited,  $S_c$ , will also increase by one to  $S_c + 1$ .

Option (2): Intra-module mode. The individual has a probability  $P_{w_i}$  of exploring a new location within the current module  $i$  or a probability  $1 - P_{w_i}$  of returning to previously visited, familiar locations. The count of movements  $n_{w_i}$  increases to  $n_{w_i} + 1$ . If a new location is explored, the count of unique locations within the module,  $S_{w_i}$ , will increment by one to  $S_{w_i} + 1$ . The exploration ends when  $S_{w_i}$  reaches the criteria of unique locations.

To validate our proposed model, we first need to estimate the parameters from empirical data. Besides the distributions of the inter-module radii of gyration  $P(R_{gc}) \sim R_{gc}^{-(1+\eta)}$  and distributions of waiting for time  $P(\Delta t)$  and jump distance  $P(\Delta r)$  (see Supplementary Information and Figs. S1), we calibrate the probability set  $P_w$ ,  $P_c$ , and  $P_{Switch}$ . The probability  $P_w$  (and  $P_c$ ) pertaining to the inclination for intra-module (inter-module) exploration is evaluated by observing changes in the number of distinct intra-module locations  $S_w$  over a span of movements  $n_w$ . As depicted in Fig.S4-S5, the relationship between  $P_w$  and  $\Delta S_w$  can be approximated as  $P_w \sim \Delta S_w = \rho_w S_w^{-\gamma_w}$ . Similarly,  $P$  and  $\Delta S$  exhibit a relationship of  $P_c \sim \Delta S = \rho_c S^{-\gamma_c}$ . It's notable that while parameter  $\gamma_w$  is nearly the same for individuals with different  $R_{gc}$ , parameter  $\gamma_c$  decreases for individuals with higher  $R_{gc}$ . When we compare the  $\gamma_w$  and  $\gamma_c$  with  $R_{gc}$  as the reference axis in Fig.2h, it becomes apparent that  $\gamma_w$  is approximately constant, while  $\gamma_c$  follows a logarithmic trend, specifically  $\gamma_c \sim -\log(R_{gc})$ . The parameters  $\rho_w$  and  $\rho_c$  are respectively estimated around 0.6 and 1, as demonstrated in Fig. S7. Furthermore, the probability  $P_{Switch}$ , which represents the tendency to transition from the current module to another module, is set to 0.14.

In cases where  $P_{Switch} = 0$ , the model simplifies to the EPR model, where all individuals only take intra-module travels such that all individuals share the same exploration tendency. See Supplementary Information and Fig. S9 for sensitivity analysis of parameters affecting model results.

**Estimating diseases spread through predicted mobility patterns.** By integrating the trajectories of all users, we can analyze the empirical cross-county fluxes and compare them with predictions

made by individual mobility models. To simulate the spread of disease based on these cross-county mobility fluxes, we utilize the meta-population susceptible–infected–recovered model<sup>37</sup>. In this model, the disease evolution within each county is governed by three states: susceptible, infectious, and removed, and the transmission of the disease between counties is described by the mobility fluxes  $T_{ij}$  from county  $j$  to county  $i$ . We select Alabama’s Augusta County as the initial outbreak location and introduce a single infection, simulating the disease’s spread over a time span of 1000 days with a reproductive number of 4, an infection rate of  $0.4 \text{ day}^{-1}$ , and cross-county migrate rate of  $0.004 \text{ day}^{-1}$ . To ensure a fair comparison, we normalize the model-predicted mobility fluxes in order to maintain the same total mobility fluxes as observed in the empirical data. The accuracy of predicting infections between empirical and model-predicted mobility fluxes is assessed using the Mean Absolute Percentage Error at each time step.

## References

1. Barbosa, H. *et al.* Human mobility: Models and applications. *Physics Reports* **734**, 1–74 (2018).
2. Gonzalez, M. C., Hidalgo, C. A. & Barabasi, A.-L. Understanding individual human mobility patterns. *Nature* **453**, 779–782 (2008).
3. Rhee, I. *et al.* On the Levy-walk nature of human mobility. *IEEE/ACM Transactions on Networking* **19**, 630–643 (2011).
4. Raichlen, D. A. *et al.* Evidence of lévy walk foraging patterns in human hunter–gatherers. *Proceedings of the National Academy of Sciences* **111**, 728–733 (2014).
5. Song, C., Qu, Z., Blumm, N. & Barabási, A.-L. Limits of predictability in human mobility. *Science* **327**, 1018–1021 (2010).
6. Schläpfer, M. *et al.* The universal visitation law of human mobility. *Nature* **593**, 522–527 (2021).
7. Song, C., Koren, T., Wang, P. & Barabási, A.-L. Modelling the scaling properties of human mobility. *Nature Physics* **6**, 818–823 (2010).
8. Pappalardo, L. *et al.* Returners and explorers dichotomy in human mobility. *Nature Communications* **6**, 1–8 (2015).
9. Zhong, L., Dong, L., Wang, Q., Song, C. & Gao, J. Universal spatial inflation of human mobility. *arXiv preprint arXiv:2406.06889* (2024).

10. Simini, F., González, M. C., Maritan, A. & Barabási, A.-L. A universal model for mobility and migration patterns. *Nature* **484**, 96–100 (2012).
11. Alessandretti, L., Sapiezynski, P., Sekara, V., Lehmann, S. & Baronchelli, A. Evidence for a conserved quantity in human mobility. *Nature Human Behaviour* **2**, 485–491 (2018).
12. Alessandretti, L., Aslak, U. & Lehmann, S. The scales of human mobility. *Nature* **587**, 402–407 (2020).
13. Xu, F., Li, Y., Jin, D., Lu, J. & Song, C. Emergence of urban growth patterns from human mobility behavior. *Nature Computational Science* **1**, 791–800 (2021).
14. Benhamou, S. Of scales and stationarity in animal movements. *Ecology Letters* **17**, 261–272 (2014).
15. Vilks, O. *et al.* Ergodicity breaking in area-restricted search of avian predators. *Physical Review X* **12**, 031005 (2022).
16. Nathan, R. *et al.* Big-data approaches lead to an increased understanding of the ecology of animal movement. *Science* **375**, eabg1780 (2022).
17. Vilks, O. *et al.* Unravelling the origins of anomalous diffusion: From molecules to migrating storks. *Physical Review Research* **4**, 033055 (2022).
18. Batty, M. Hierarchy in cities and city systems. *Hierarchy in Natural and Social Sciences* 143–168 (2006).



19. Louf, R. & Barthélemy, M. Modeling the polycentric transition of cities. *Physical Review Letters* **111**, 198702 (2013).
20. Sahasrabuddhe, R., Lambiotte, R. & Alessandretti, L. From centre to centres: polycentric structures in individual mobility. *arXiv preprint arXiv:2108.08113* (2021).
21. Cabrera-Arnau, C., Zhong, C., Batty, M., Silva, R. & Kang, S. M. Inferring urban polycentricity from the variability in human mobility patterns. *Scientific Reports* **13**, 5751 (2023).
22. Clauset, A., Newman, M. E. & Moore, C. Finding community structure in very large networks. *Physical Review E—Statistical, Nonlinear, and Soft Matter Physics* **70**, 066111 (2004).
23. Newman, M. E. Modularity and community structure in networks. *Proceedings of the National Academy of Sciences* **103**, 8577–8582 (2006).
24. Frank, L. D. & Engelke, P. O. The built environment and human activity patterns: Exploring the impacts of urban form on public health. *Journal of Planning Literature* **16**, 202–218 (2001).
25. Belik, V., Geisel, T. & Brockmann, D. Natural human mobility patterns and spatial spread of infectious diseases. *Physical Review X* **1**, 011001 (2011).
26. Chang, S. *et al.* Mobility network models of COVID-19 explain inequities and inform reopening. *Nature* **589**, 82–87 (2021).
27. Althoff, T. *et al.* Large-scale physical activity data reveal worldwide activity inequality. *Nature* **547**, 336–339 (2017).

28. Wang, Q., Phillips, N. E., Small, M. L. & Sampson, R. J. Urban mobility and neighborhood isolation in America's 50 largest cities. *Proceedings of the National Academy of Sciences* **115**, 7735–7740 (2018).
29. Athey, S., Ferguson, B., Gentzkow, M. & Schmidt, T. Estimating experienced racial segregation in US cities using large-scale GPS data. *Proceedings of the National Academy of Sciences* **118**, e2026160118 (2021).
30. Golan, Y. & Sherman, E. Resolving mixed mechanisms of protein subdiffusion at the T cell plasma membrane. *Nature Communications* **8**, 1–15 (2017).
31. Meekan, M. G. *et al.* The ecology of human mobility. *Trends in Ecology & Evolution* **32**, 198–210 (2017).
32. De Montjoye, Y.-A., Smoreda, Z., Trinquart, R., Ziemlicki, C. & Blondel, V. D. D4D-Senegal: The second mobile phone data for development challenge. *arXiv preprint arXiv:1407.4885* (2014).
33. Aslak, U. & Alessandretti, L. Infostop: Scalable stop-location detection in multi-user mobility data. *arXiv preprint arXiv:2003.14370* (2020).
34. Miller, H. J. Tobler's first law and spatial analysis. *Annals of the Association of American Geographers* **94**, 284–289 (2004).
35. Barabási, A.-L. *Network Science* (Cambridge University Press, 2014).
36. Fortunato, S. Community detection in graphs. *Physics Reports* **486**, 75–174 (2010).

37. Brockmann, D. & Helbing, D. The hidden geometry of complex, network-driven contagion phenomena. *Science* **342**, 1337–1342 (2013).

**Acknowledgments** We thank Jinzhu Yu for his assistance with pre-processing the Senegal mobility data and fruitful discussion. J.G. and L.Z. acknowledge the support of the US National Science Foundation under Grant No. 2047488. L.D. was supported by the National Natural Science Foundation of China under Grant No. 42422110 and the Fundamental Research Funds for the Central Universities, Peking University.

**Author contributions** L.Z., L.D., Q.W., and J.G. conceived the project and designed the experiments; Q.W. collected and analyzed the US data; L.Z. analyzed the Senegal data; L.Z., L.D., J.G., and C.S. carried out theoretical calculations and performed the experiments; all authors wrote and edited the manuscript.

**Competing interests** The authors declare no competing interests.

**Correspondence and requests for materials** should be addressed to J.G.

**Additional information** Supplementary Notes 1-4, including Supplementary Figures 1-11, and Supplementary Tables 1-3.

**Data and code availability** Data files and the Python script have been deposited in <https://github.com/lucinezh>

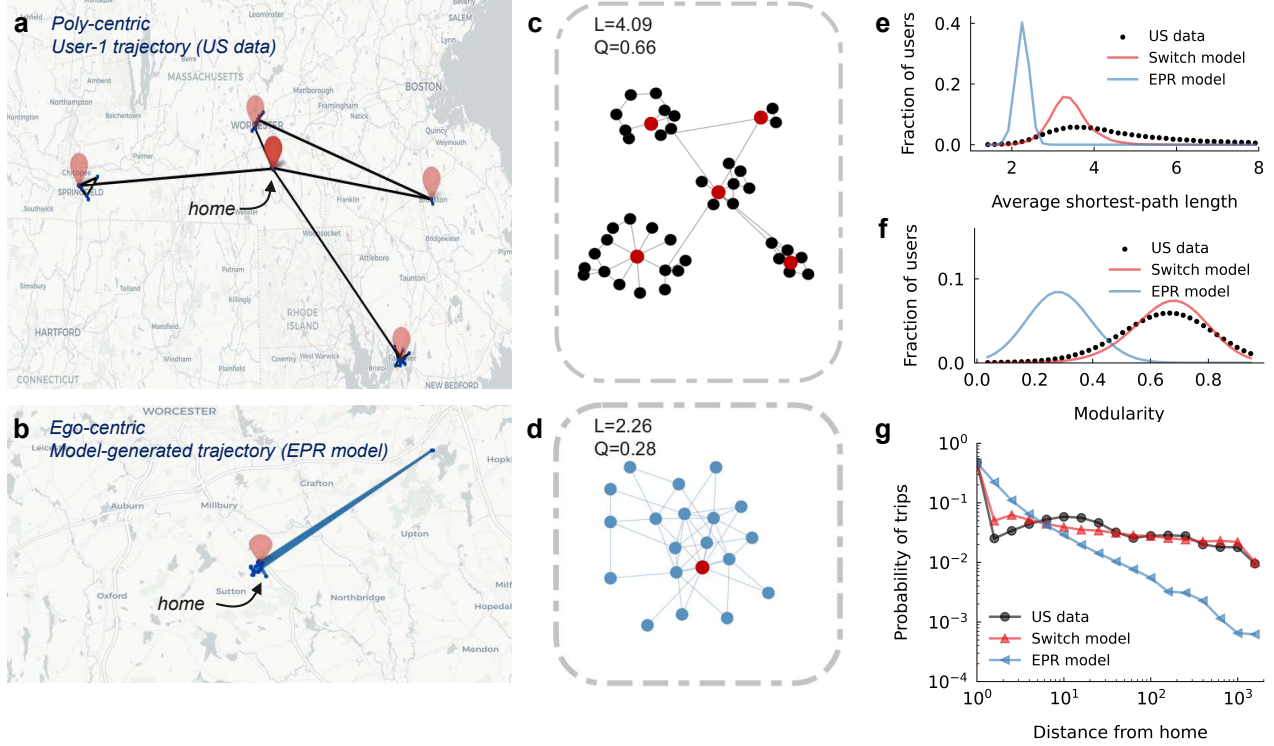


**Figure 1: The polycentric modular structure of human mobility network.** (a, b) Trajectory of the anonymous cell phone user exhibits polycentricity, as opposed to the egocentricity of trajectory generated by a traditional model. The red marker denotes the center of activity. (c, d) Mobility networks associated with trajectories in (a, b). The mobility networks are constructed regarding trajectory sequence and spatial distance, where nodes represent stay points and edges represent recorded travels. (e) The average shortest-path length distribution of users' mobility networks. (f) The geometric modularity distribution of users' mobility networks. (g) Probability of trips at a distance with the home as the reference point. The polycentric nature leads empirical mobility networks of high shortest-path length and high modularity and also have numerous travels distant from home. While the egocentric model, like the EPR model, fails to capture the network properties and generate distant travels. Our proposed model aligns with real-world mobility data and networks.

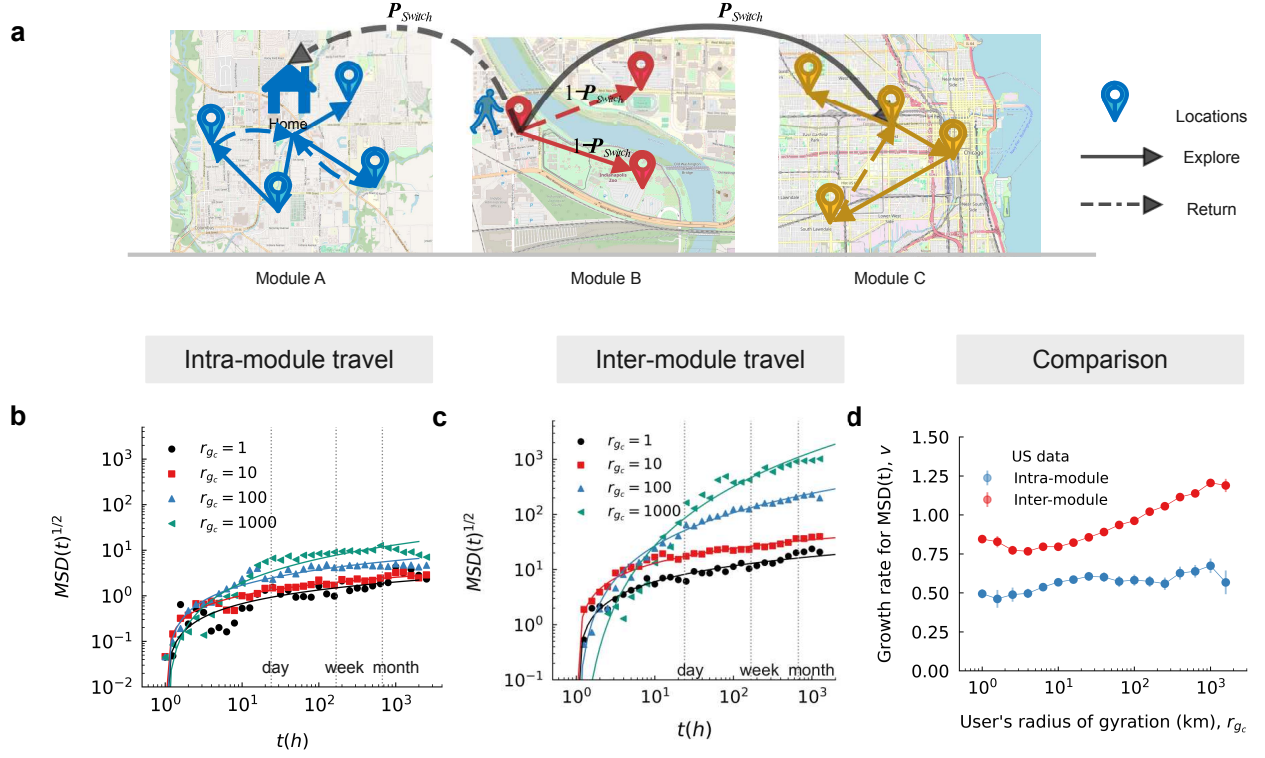


Figure 2: **The switch of exploration modes within and across modules.** (a) Illustration of the switch from intra-module travel mode to inter-module travel mode. (b,c) The time evolution of the mean squared displacement,  $MSD(t)$ , is used to quantify the spatiotemporal dynamics of inter- and intra-module mobility, where  $MSD(t)^{1/2} \sim \log(t)^v$ . (d) The growth rate  $v$  is plotted with error bars for users with different values of  $R_{gc}$ . Despite variations in users'  $R_{gc}$ , the analysis shows a lower growth rate  $v$  for intra-module travels compared to inter-module travels, indicating a reduced tendency for exploration within modules.

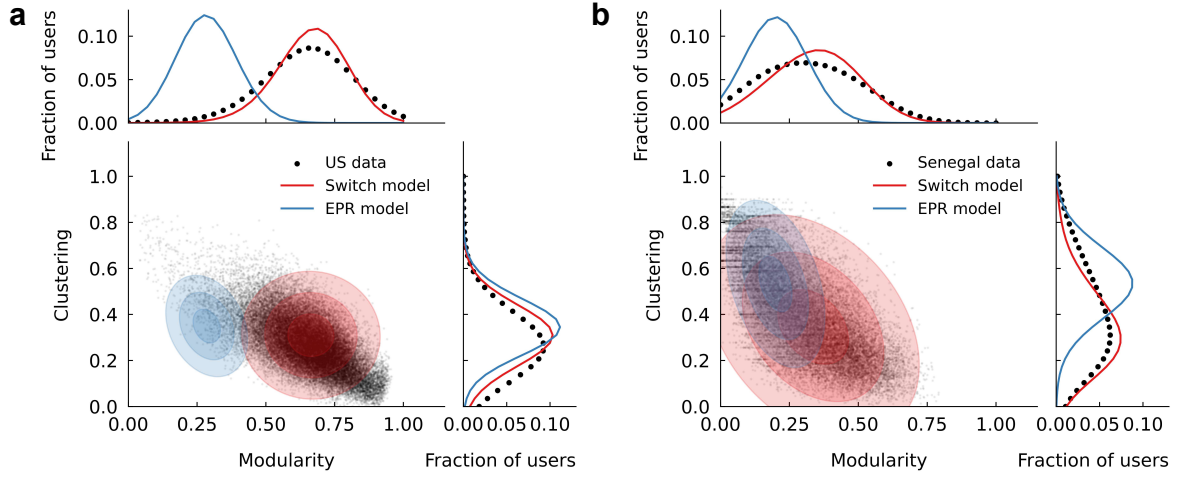


Figure 3: **Switch mechanism depicts the modular structures in mobility networks.** (a, b) The unusual inverse relationship between modularity and the clustering coefficient of mobility networks in U.S. data (a) and Senegal data (b). The polycentric switch model captures the inverse relationship, effectively generating a network structure with spatially separated modules but a limited number of triangle paths, aligning with empirical data.

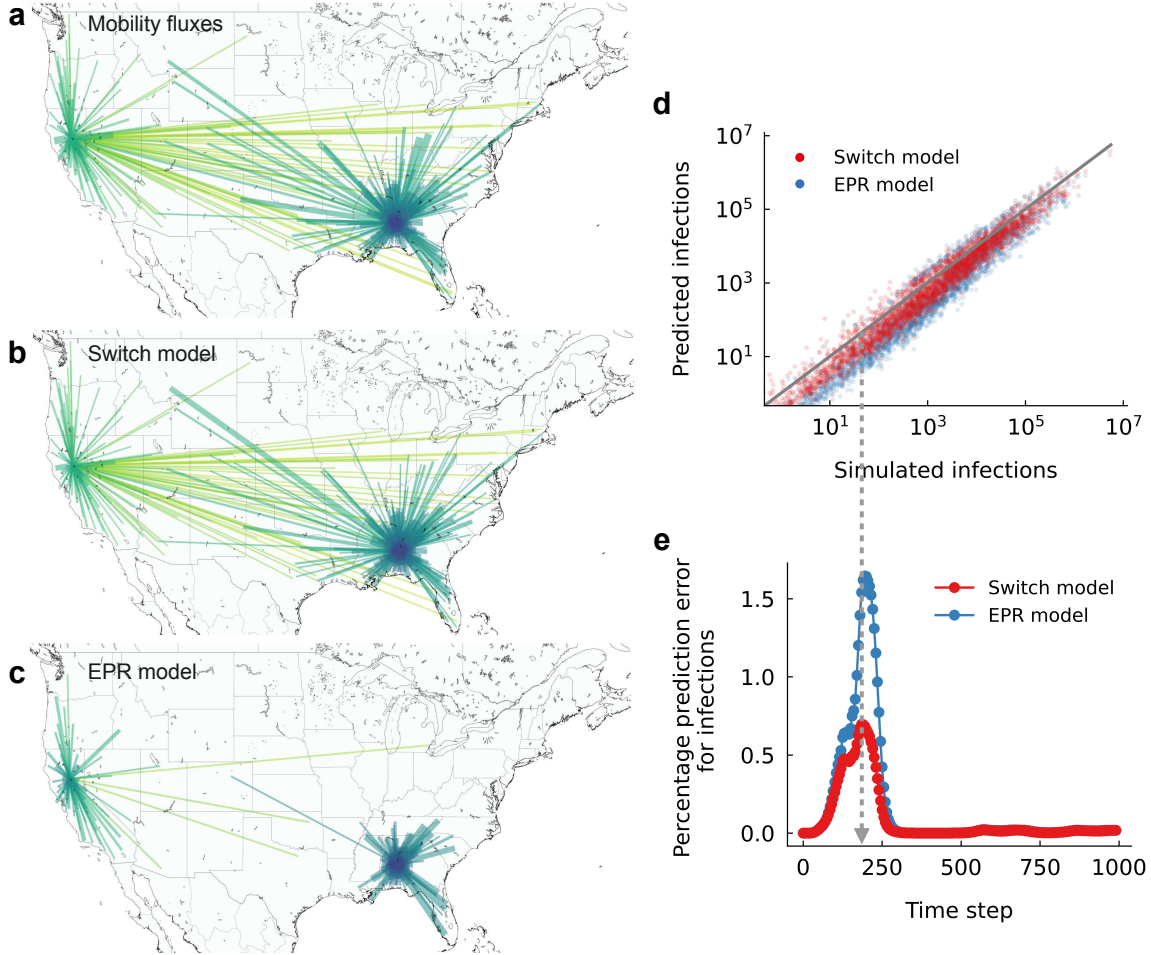
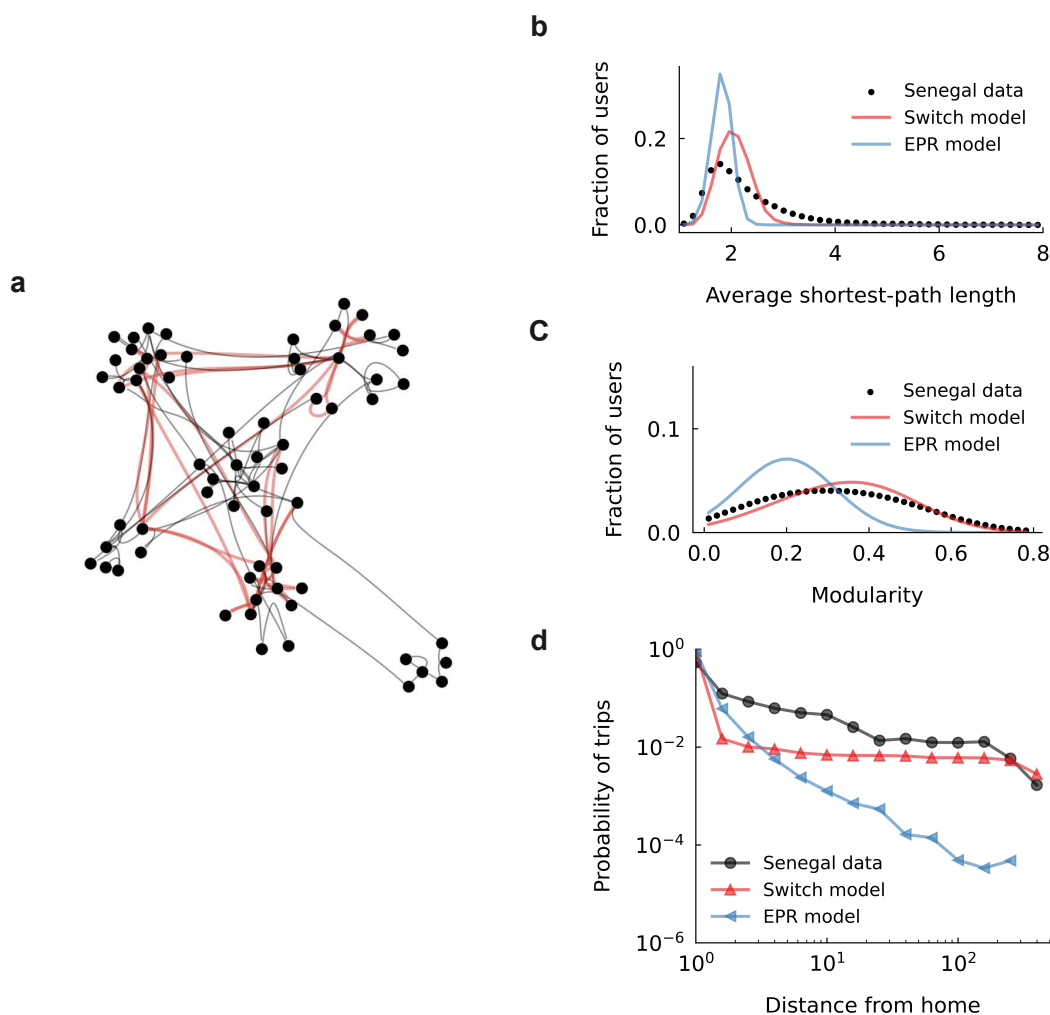


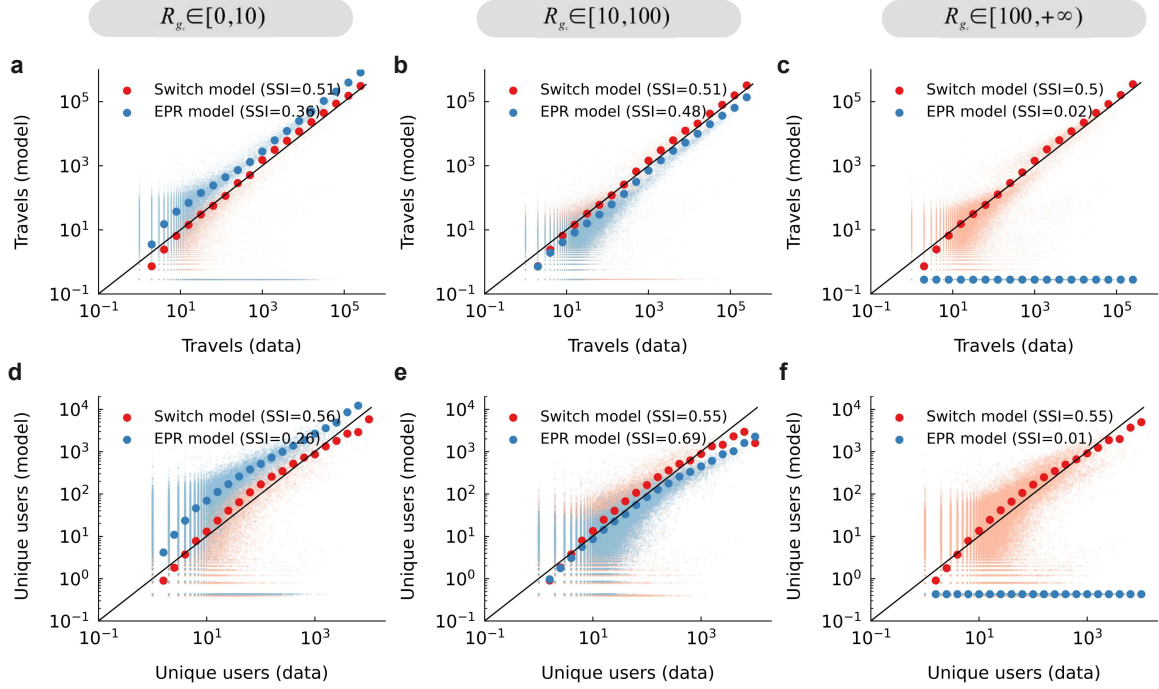
Figure 4: **Switch mechanism predicts long-range travels and infections.** (a, b, c) The mobility flux originates from two counties (located in Alabama and California, respectively). The switch model demonstrates superior alignment with data, particularly in generating long-range fluxes. While the egocentric EPR model generates fewer long-range fluxes. To evaluate the models' efficacy in predicting infections, we simulate the spread of disease on predicted and empirical cross-county fluxes, with an initial outbreak in Alabama County. (d) The comparison between model-predicted infections and simulated infections in all counties at the snapshot time  $t = 150$ . (e) Models' prediction error at the entire time course. The switch model demonstrates low prediction error, indicating its proficiency in accurately predicting infections.



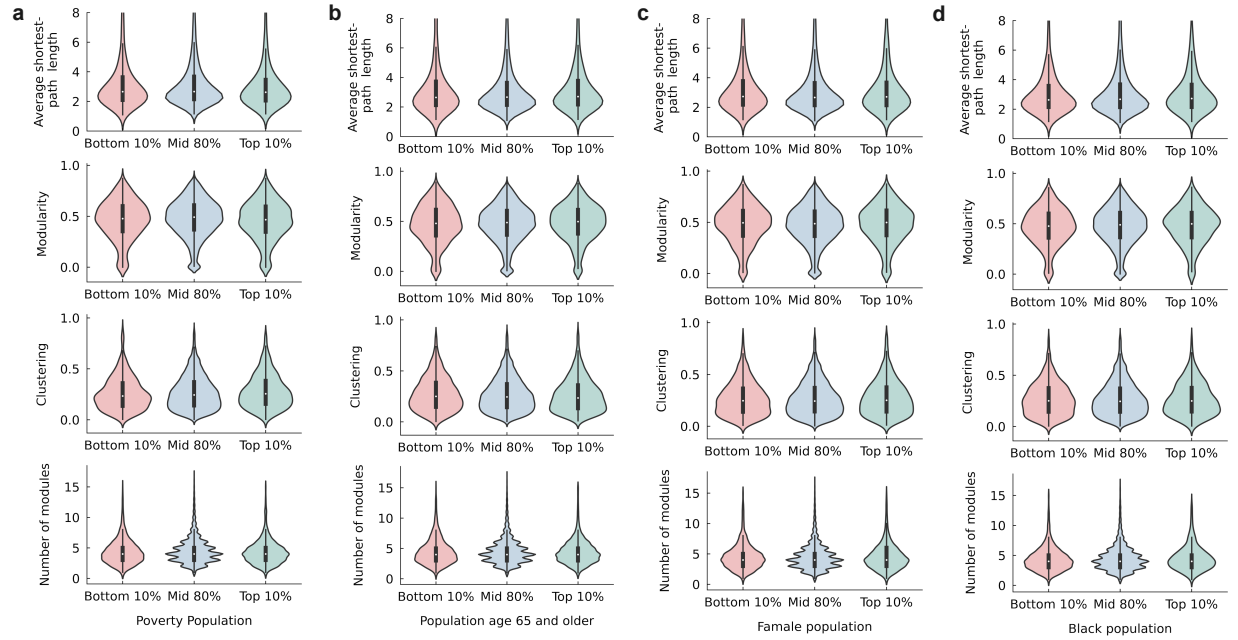
## Extended Data Figures



**Extended Data Fig. 1: Mobility network associated with trajectories for Senegal data.** (a) Visualizations of example trajectory networks. Edges are in black but triangle links are in red. (b) The average shortest-path length distribution of users' mobility networks. (c) The geometric modularity distribution of users' mobility networks. (d) Probability of trips at a distance with the home as the reference point. Same as Fig.1, the egocentric EPR model fails to fit with real-world data. The distribution of real-world lengths of the shortest path shows a long-tail pattern, and the extent of geometric modularity is more significant.



**Extended Data Fig. 2: The switch mechanism better depicts collective mobility.** Model-predicted and empirical data of mobility fluxes (a, b, c) and unique users (d, e, f) between counties are compared in three user groups with  $R_{gc}$  in ranges  $[0, 10]$ ;  $[10, 100]$ ;  $[100, \infty]$ . A higher SSI means a better match with empirical data. The egocentric EPR model overestimates the travel for user groups in  $R_{gc} \in [0, 10]$  that primarily have small-distance travels. The polycentric switch model fits better with data with higher SSI for all user groups.



**Extended Data Fig. 3: Mobility network characteristics across diverse populations in different demographic attributes.** When categorizing users based on the proportions of the poverty population in their home locations **(a)**, the elderly population (age 65 and older) **(b)**, the female population **(c)**, and the black population **(d)**, the distribution of average shortest path length, clustering, modularity, and module numbers remain consistent across user groups. The median values are indicated in white.